Fluid particle diffusion in a semidilute suspension of model micro-organisms

Takuji Ishikawa,[1] J. T. Locsei,[2] and T. J. Pedley[2]
[1]*Department of Bioengineering and Robotics, Tohoku University, 6-6-01 Aoba, Aramaki, Aoba-ku, Sendai 980-8579, Japan*
[2]*Department of Applied Mathematics and Theoretical Physics, University of Cambridge, Centre for Mathematical Sciences, Wilberforce Road, Cambridge CB3 0WA, United Kingdom*
(Received 23 January 2010; revised manuscript received 26 May 2010; published 27 August 2010)

We calculate non-Brownian fluid particle diffusion in a semidilute suspension of swimming micro-organisms. Each micro-organism is modeled as a spherical squirmer, and their motions in an infinite suspension otherwise at rest are computed by the Stokesian-dynamics method. In calculating the fluid particle motions, we propose a numerical method based on a combination of the boundary element technique and Stokesian dynamics. We present details of the numerical method and examine its accuracy. The limitation of semidiluteness is required to ensure accuracy of the fluid particle velocity calculation. In the case of a suspension of non-bottom-heavy squirmers the spreading of fluid particles becomes diffusive in a shorter time than that of the squirmers, and the diffusivity of fluid particles is smaller than that of squirmers. It is confirmed that the probability density distribution of fluid particles also shows diffusive properties. The effect of tracer particle size is investigated by inserting some inert spheres of the same radius as the squirmers, instead of fluid particles, into the suspension. The diffusivity for inert spheres is not less than one tenth of that for fluid particles, even though the particle size is totally different. Scaling analysis indicates that the diffusivity of fluid particles and inert spheres becomes proportional to the volume fraction of squirmers in the semidilute regime provided that there is no more than a small recirculation region around a squirmer, which is confirmed numerically. In the case of a suspension of bottom-heavy squirmers, horizontal diffusivity decreases considerably even with small values of the bottom heaviness, which indicates the importance of bottom heaviness in the diffusion phenomena. We believe that these fundamental findings will enhance our understanding of the basic mechanics of a suspension of swimming micro-organisms.

DOI: 10.1103/PhysRevE.82.021408 PACS number(s): 83.80.Hj, 87.19.U−, 87.19.ru, 66.10.cg

I. INTRODUCTION

Mass transport in a suspension of micro-organisms is important in a wide variety of biological phenomena, for instance, nutrient absorption in the intestines where enteric bacteria stir nutrients, oxygen transport in harmful red tides in coastal regions of the ocean, mass transport in a bioreactor, and so on. Some micro-organisms show chemotaxis and swim toward higher concentrations of attractive chemical substances. Mass transport in such a suspension plays an important role in the bulk motion of cells. Micro-organisms consume nutrients and oxygen in a suspension, which strongly affects their growth and reproduction rates. The consumption rate of nutrients may be influenced by the micron-scale flow field generated by cells' swimming motion, because the Péclet number for the nutrient transport is sometimes larger than unity. In such a case the consumption rate is no longer linearly related to the volume fraction of cells, and hydrodynamic interaction between cells becomes crucial when the suspension is not sufficiently dilute [1].

A suspension of micro-organisms is often modeled as a continuum in which the variables are volume-averaged quantities [2–4], because the size of individual micro-organisms is often much smaller than that of the flow field of interest. Continuum models have also been proposed for the analysis of phenomena such as bioconvection [5–9]; however, these former models neglected the effect of the micro-organisms on the diffusivity of the cells themselves as well as of chemical substances. A governing equation for mass transport of chemical substances in a continuum model may be given as [10]

$$\frac{\partial \phi}{\partial t} = -\nabla \cdot (\phi \boldsymbol{v} - D \nabla \phi) - q_{cell}, \tag{1}$$

where ϕ is the concentration of the chemical substance, t is the time, $\boldsymbol{v}$ is the velocity of the suspension, D is the diffusivity, and q_{cell} is the rate of consumption by cells. In most former studies, D was assumed to be equivalent to Brownian diffusivity. In practice, however, D must be increased by introducing the cells' swimming motion, because the cells stir the surrounding fluid. The magnitude of the increase in D can be calculated by tracking the motions of individual chemical particles in the suspension for a long enough time period.

The diffusivity of inert particles in a cell suspension was first investigated experimentally by Wu and Libchaber [11]. They drew a stable two-dimensional soap film and seeded bacteria (*Escherichia coli*) and micron-scale polystyrene beads in it. They investigated the effect of bacterial motion on the diffusivity of micron-scale beads in a freely suspended film. Their results revealed superdiffusion over short times whereas normal diffusion appeared after a long enough time. Kim and Breuer [12] used *E. coli* to experimentally investigate the enhanced diffusion of large molecules in a bacterial suspension. They found that the effective diffusion coefficient increased linearly as the cell concentration increased. Since they used a rather small volume fraction of bacteria, collective behavior would not have appeared, and the results were different from those of Wu and Libchaber [11]. Most recently, Leptos *et al.* [13] experimentally investigated diffusion of passive tracers in suspensions of eukary-

 ©2010 The American Physical Society

otic swimmers, the alga *Chlamydomonas reinhardtii*. They reported that the tracers behave diffusively, with a time-dependent but self-similar probability distribution function of displacements consisting of a Gaussian core and robust exponential tails.

Some numerical investigations have also been reported. Hernandes-Ortiz *et al.* [14] and Underhill *et al.* [15] performed direct simulations of large populations of confined hydrodynamically interacting swimming particles and investigated the diffusion of tracer particles in the suspension. Saintillan and Shelley [16,17] used a nonlinear kinetic theory and computed the fluid mixing in a suspension of self-propelled particles. Although these results are suggestive and consistent with former experimental results, these authors did not solve the near-field hydrodynamics precisely. Llopis and Pagonabarraga [18,19] employed a lattice Boltzmann method to analyze the collective dynamics of self-propelling particles and the velocity field of the solvent fluid. Although the lattice Boltzmann method is efficient to calculate motions of many particles, the resolution of flow field is restricted by the distance between lattice points d_{LP}. In most of their simulation cases, a particle radius of $2.5d_{LP}$ was used, and the flow field between two nearby particles was not accurately calculated. The low resolution in calculating the flow field leads to inaccurate prediction of the lubrication forces between particles. In calculating near-field fluid dynamics accurately, one needs to employ a high-resolution numerical method between two nearby surfaces. We can say that the details of diffusion in a suspension of micro-organisms are still not well understood. Experimentally, tracking small particles continuously in a suspension of large micro-organisms is very difficult in the nondilute regime, but no suitable numerical method to address this problem has yet been proposed.

There are some methods that can efficiently simulate a concentrated suspension of particles. Ladd [20–22] was able to carry out dynamic simulations of suspensions with up to 32 000 spheres by a lattice Boltzmann method. Sangani and Mo [23] developed a fast multipole method. They carried out dynamic simulations of suspensions with up to 8000 spheres and concluded that accurate results were obtained even when the order to which the multipole series is expanded and the order of the field induced by the individual particles are equal. Zinchenko and Davis [24–27] improved the standard boundary element method (BEM) and were able to simulate up to 200 deformable drops in a simple shear flow. A high efficiency of the method was demonstrated, with two orders of magnitude gains over the standard boundary element method. Those numerical methods are all efficient in simulating particle motions in a suspension. However, none of them have been applied to calculate the motions of infinitesimal fluid elements in a suspension.

Here, we calculate fluid particle diffusion in a suspension of micro-organisms. The model micro-organism used in this paper is the same as the one used by Ishikawa *et al.* [28] and will be referred to as a *squirmer*. Details of a spherical squirmer will be explained in Sec. II A. The three-dimensional movement of identical squirmers in a fluid otherwise at rest is computed, for random initial positions and orientations, by the Stokesian-dynamics method (SDM) developed by Ishikawa *et al.* [29,30] (cf. Sec. II B). The infinite extent of the suspension is realized by assuming periodic boundary conditions. Fluid particles are assumed to be infinitely small but do not show any Brownian motion, i.e., they are ideal Lagrangian particles moving with the fluid velocity, although real fluids, such as water, show self-diffusion due to Brownian motion [31]. This treatment corresponds to infinitely large Péclet number flow for the fluid particles. In order to solve the fluid particle motions, we propose a numerical method based on a BEM [32] and the SDM [29,30]. This method is a modified version of our previous method for a suspension of inert spheres [32], but here we need to take into account the squirming motion on the spherical surfaces. The details of the method will be presented in Sec. II C. The accuracy of the numerical method is checked in Sec. III by comparing the velocity fields obtained by the present method and the exact solution (or that obtained using BEM). In Sec. IV, the diffusive behavior of fluid particles in a semidilute suspension of *non-bottom-heavy* squirmers will be investigated. The effects of volume fraction on the diffusive properties will be demonstrated and the scaling of the results will be discussed. The effect of tracer particles' size will also be investigated by introducing some inert spheres, instead of fluid particles, into the suspension. In Sec. V, the diffusive behavior of fluid particles in a semidilute suspension of *bottom-heavy* squirmers will be investigated.

II. BASIC EQUATIONS AND NUMERICAL METHODS

The Stokesian-dynamics simulation method for computing the hydrodynamic interactions among an infinite suspension of squirmers, in the absence of Brownian motion and at negligible particle Reynolds number, was developed by Ishikawa *et al.* [29] on the basis of former studies on inert spheres [33,34]. The numerical methods for squirmer motions are the same as in [29], so only a brief explanation will be made. Fluid particles are assumed to be infinitely small Lagrangian particles, following the flow precisely. In a previous study [32], we proposed a numerical method based on the BEM and the SDM for calculating fluid particle motions in a sheared suspension of inert spheres. The numerical method introduced here is a modified version of our previous method, so that we can take into account the squirming motion on the spherical surfaces. The numerical methods for simulating squirmer motions are valid even for a concentrated suspension of squirmers, whereas those for fluid particle motions are valid only in a semidilute regime.

A. Squirmer

The model micro-organism (a spherical squirmer) is assumed to be neutrally buoyant (i.e., force free), possibly bottom heavy (therefore not necessarily torque free) and non-Brownian, and to swim at very small Reynolds number (i.e., it is inertia free). The model of a squirmer was first proposed by Lighthill [35] and has been extended by Blake [36], Felderhof and Jones [37], and Stone and Samuel [38]. The model has also been used by Magar *et al.* [39,40] to analyze nutrient uptake properties of a solitary squirmer.

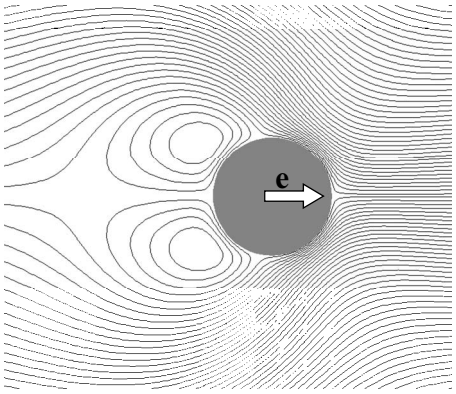

FIG. 1. Streamlines relative to the squirmer center (β=5). Streamlines are drawn at 0.1 interval, and uniform flow comes from far right.

The sphere's surface is assumed to move purely tangentially and these tangential motions are assumed to be axisymmetric and time independent. Thus, the tangential surface velocity on a squirmer is given as

$$\boldsymbol{u}_s = \sum_{n=1}^{2} \frac{2}{n(n+1)} B_n \left(\frac{\boldsymbol{e}\cdot\boldsymbol{r}}{r}\frac{\boldsymbol{r}}{r} - \boldsymbol{e} \right) P_n'(\boldsymbol{e}\cdot\boldsymbol{r}/r), \tag{2}$$

where P_n is the nth Legendre polynomial, $\boldsymbol{e}$ is the unit orientation vector of a squirmer, $\boldsymbol{r}$ is the position vector, and $r=|\boldsymbol{r}|$. We will follow [28] and omit squirming modes higher than the second (i.e., $B_n=0$ in $\boldsymbol{u}_s$ when $n\geq 3$), although such a restriction is not required for the numerical methods to work. The swimming speed of a solitary squirmer is $U_{sol}=2B_1/3$. We denote by β the ratio of second mode squirming to first mode squirming, i.e., $\beta=B_2/B_1$. It should be noted that B_2, and hence β, can have either sign. A squirmer with positive β is a *puller*, analogous to a micro-organism for which the thrust-generating apparatus is in front of the body (which provides the drag), as for biflagellate algae such as *Chlamydomonas*, whereas a squirmer with negative β is a *pusher*, i.e., the thrust is generated behind the body, as for bacteria or spermatozoa. Streamlines for the case β=5 are shown in Fig. 1, as an example. We note that recirculation regions occur when $|\beta|>1$.

B. Equations for squirmer motion

At negligible particle Reynolds number, motions of N squirmers periodically replicated in three-dimensional space can be given as [29]

$$\begin{pmatrix} \boldsymbol{F} \\ \boldsymbol{L} \\ \boldsymbol{S} \end{pmatrix} = [\boldsymbol{R}^{far} - \boldsymbol{R}_{2B}^{far} + \boldsymbol{R}_{2B}^{near}] \begin{pmatrix} \boldsymbol{U} - \langle \boldsymbol{u} \rangle \\ \boldsymbol{\Omega} - \langle \omega \rangle \\ -\langle \boldsymbol{E} \rangle \end{pmatrix} + [\boldsymbol{R}^{far} - \boldsymbol{R}_{2B}^{far}] \begin{pmatrix} -\frac{2}{3}B_1\boldsymbol{e} + \boldsymbol{Q}_{sq} \\ 0 \\ -\frac{1}{5}B_2(3\boldsymbol{ee} - \boldsymbol{I}) \end{pmatrix} + \begin{pmatrix} \boldsymbol{F}_{sq}^{near} \\ \boldsymbol{L}_{sq}^{near} \\ \boldsymbol{S}_{sq}^{near} \end{pmatrix}, \tag{3}$$

where $\boldsymbol{F}$, $\boldsymbol{L}$, and $\boldsymbol{S}$ are, respectively, the force, torque, and stresslet a squirmer exerts on the fluid. $\boldsymbol{U}$ and $\boldsymbol{\Omega}$ are the translational and rotational velocities of a squirmer, $\boldsymbol{I}$ is the unit tensor, and $\boldsymbol{Q}_{sq}$ is the far-field contribution of the irreducible quadrupole due to squirming motion. $\boldsymbol{R}^{far}$ is the far-field contribution to the grand resistance matrix, which is the inverse of the far-field contribution to the grand mobility matrix, i.e., $\boldsymbol{R}^{far}=\{\boldsymbol{M}^{far}\}^{-1}$. $\boldsymbol{M}^{far}$ is derived from the Faxén laws for the force, torque, and stresslet for a squirmer, in which the disturbed flow field is expressed in terms of the multipole expansion of other squirmers. The infinite extent of the suspension is taken into account by using Ewald summation [41]. As discussed by Durlofsky *et al.* [42] inverting the Ewald-summed mobility matrix sums an infinite number of reflected interactions among an infinite number of particles, so it is a true many-body approximation to the resistance matrix. This method is, therefore, applicable to any volume fraction of particles. $\boldsymbol{R}^{far}$ still lacks near-field interactions, because they are reproduced only when all multipoles are included. In order to include the near-field interactions, we follow the method of Durlofsky *et al.* [42] and add near-field multipoles in a pairwise additive fashion; $\boldsymbol{R}_{2B}^{far}$ is the far-field two-body resistance matrix and $\boldsymbol{R}_{2B}^{near}$ is the near-field two-body resistance matrix, which can be found in standard texts such as by Kim and Karrila [43]. $\boldsymbol{F}_{sq}^{near}$, $\boldsymbol{L}_{sq}^{near}$, and $\boldsymbol{S}_{sq}^{near}$ are, respectively, the force, torque, and stresslet generated by the two-squirmer interaction in the near fluid. We have already compiled a database of pairwise interactions of squirmers [28], so we will use the database in constructing these multipoles. The first matrix multiplication on the right-hand side (RHS) of Eq. (3) indicates the contribution from two inert spheres with translational and rotational velocities in a linear flow field, which is equal to the equation derived by [34]. The second matrix multiplication indicates the far-field contribution from the squirming motion, and the last term indicates the near-field contribution from the squirming motion.

If squirmers are bottom heavy, external gravitational torques are generated when they are not oriented vertically, and they tend to swim upward on average. If the distance of the center of gravity is l from the center of the squirmer, in the opposite direction to its swimming direction in undisturbed fluid, then there is an additional torque of

$$\boldsymbol{L}_{bh} = \tfrac{4}{3}\pi a^3 \rho l \boldsymbol{e} \wedge \boldsymbol{g}, \tag{4}$$

where ρ is the cell density, $\boldsymbol{g}$ is the gravitational acceleration vector, and the gravitational direction is $\boldsymbol{g}/g$.

A nonhydrodynamic short-range repulsive force between squirmers, $\boldsymbol{F}_{rep}$, is added to the system in order to avoid the prohibitively small time step needed to overcome the problem of overlapping squirmers. We will follow Brady and Bossis [44] and Ishikawa *et al.* [29], and use the following function:

$$\boldsymbol{F}_{rep} = \alpha_1 \frac{\alpha_2 \exp(-\alpha_2\varepsilon)}{1-\exp(-\alpha_2\varepsilon)} \frac{\boldsymbol{r}}{r}, \tag{5}$$

where α_1 is a dimensional coefficient, α_2 is a dimensionless coefficient, and ε is the minimum separation between squirmer surfaces nondimensionalized by their radius. The coefficients used in this study are $\alpha_1=0.1$ and $\alpha_2=10^3$. The

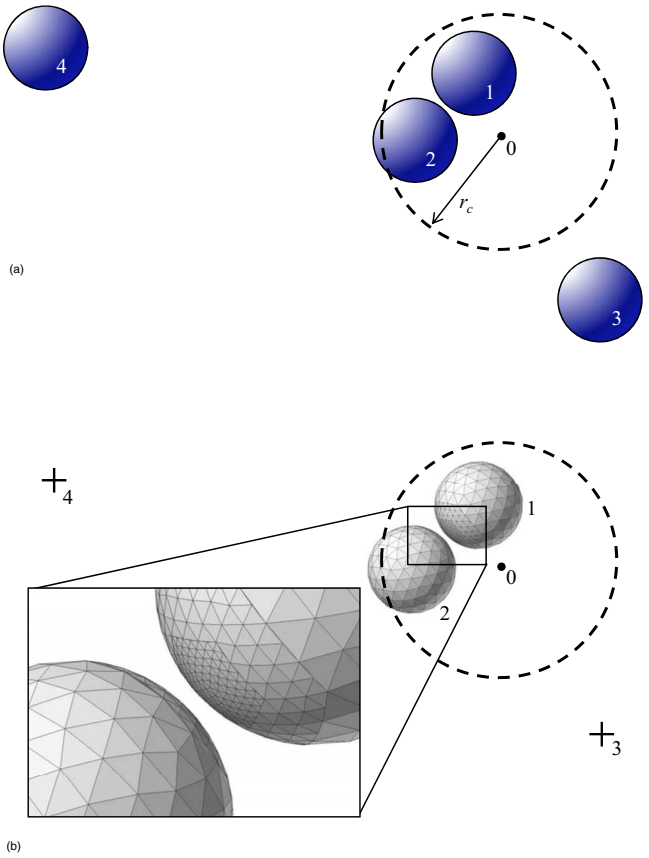

FIG. 2. (Color online) Configuration of particles and the computational mesh for a fluid particle motion. (a) Schematics of the configuration of squirmers around a fluid particle at point 0. Inside the broken line indicates the near field from the fluid particle. (b) Computational mesh for a fluid particle motion. In calculating the far-field contribution, the first few multipoles are considered at + points, i.e., points 3 and 4. In calculating the near-field contribution, a triangular mesh is generated on spherical surfaces 1 and 2 for BEM computations. The finer mesh is generated in the near-contact region.

minimum separation obtained with these parameters is about 10^{-4}. We have not used any repulsive forces between a squirmer and a fluid particle, because the velocity on a squirmer surface is given as a boundary condition by Eq. (2), which does not permit a fluid particle to penetrate into the squirmer. The reliability of the described numerical methods has been confirmed in [29].

C. Equations for fluid particle motion

If a suspension is in the *semidilute* regime, most of the interactions between squirmers are pairwise. Thus, one can assume that a fluid particle may have two squirmers in its near field but the other squirmers are in the far field as shown in Fig. 2(a), where squirmers 1 and 2 are in the near field. The probability for a fluid particle to have one squirmer in its near field is of $\mathcal{O}(c)$, where c is the volume fraction of squirmers. The probability for a fluid particle to have two squirmers in its near field is of $\mathcal{O}(c^2)$, and to have three squirmers is of $\mathcal{O}(c^3)$. In this study, the maximum number of squirmers in the near field is assumed to be two, which defines *semidiluteness*.

The flow field external to N squirmers periodically replicated in three-dimensional space can be given in integral form by [45]

$$u_i(\boldsymbol{x}) - \langle u_i(\boldsymbol{x})\rangle = -\frac{1}{8\pi\mu}\sum_{\alpha=1}^{N}\int_{A_\alpha} J_{ij}(\boldsymbol{x}-\boldsymbol{y})q_j(\boldsymbol{y})dA_y, \quad (6)$$

where $\boldsymbol{u}$ is the velocity, $\boldsymbol{q}$ is the single-layer potential, and A is the surface of a particle. The angular brackets $\langle\ \rangle$ indicate the suspension average. $\boldsymbol{J}$ is evaluated by Ewald summation on the lattice and reciprocal lattice of image points, as derived by Beenakker [41]:

$$J_{ij}(\boldsymbol{r}) = \sum_{\gamma} H_{ij}^{(1)}(\boldsymbol{r}_\gamma) + \frac{8\pi}{V}\sum_{\lambda\neq 0}[H_{ij}^{(2)}(\boldsymbol{k}_\lambda)\cos(\boldsymbol{k}_\lambda\cdot\boldsymbol{r})] - \frac{8\xi}{\sqrt{\pi}}\delta_{ij}\delta(\boldsymbol{r}), \quad (7)$$

$$H_{ij}^{(1)}(\boldsymbol{r}) = \frac{\delta_{ij}}{r}\left\{\mathrm{erfc}(\xi r) + \frac{e^{-\xi^2 r^2}}{\sqrt{\pi}}(4\xi^3 r^3 - 6\xi r)\right\} + \frac{r_i r_j}{r^3}\left\{\mathrm{erfc}(\xi r) + \frac{e^{-\xi^2 r^2}}{\sqrt{\pi}}(2\xi r - 4\xi^3 r^3)\right\},$$

$$H_{ij}^{(2)}(\boldsymbol{k}) = \left(\frac{\delta_{ij}}{|\boldsymbol{k}|^2} - \frac{k_i k_j}{|\boldsymbol{k}|^4}\right)\left(1 + \frac{|\boldsymbol{k}|^2}{4\xi^2} + \frac{|\boldsymbol{k}|^4}{8\xi^4}\right)\exp\left(-\frac{|\boldsymbol{k}|^2}{4\xi^2}\right), \quad (8)$$

where ξ is the convergence parameter, $\boldsymbol{\delta}$ is the unit isotropic tensor, V is the volume of each unit cell, and $r=|\boldsymbol{r}|$. The lattice points are $\boldsymbol{x}_\gamma$ and $\boldsymbol{r}_\gamma=\boldsymbol{r}-\boldsymbol{x}_\gamma$; $\boldsymbol{k}_\lambda$ are the reciprocal lattice vectors defined such that $\boldsymbol{x}_\gamma\cdot\boldsymbol{k}_\lambda$ is an integer multiple of 2π. The first sum in the RHS of Eq. (7) converges rapidly in real space, while the second converges rapidly in reciprocal space.

The RHS of Eq. (6) can be expanded in moments about the center of each particle with radius a as [42]

$$u_i(\boldsymbol{x}) - \langle u_i(\boldsymbol{x})\rangle = \frac{1}{8\pi\mu}\sum_{\alpha=1}^{N}\left[\left(1+\frac{a^2}{6}\nabla^2\right)J_{ij}F_j^\alpha + R_{ij}L_j^\alpha + \left(1+\frac{a^2}{10}\nabla^2\right)K_{ijk}S_{jk}^\alpha + \nabla_k\nabla_l J_{ij}Q_{klj}^\alpha + \cdots\right], \quad (9)$$

where $\boldsymbol{F},\boldsymbol{L},\boldsymbol{S},\boldsymbol{Q}$ are, respectively, the monopole, the antisymmetric dipole, the symmetric dipole, and the irreducible quadrupole of the single-layer potential. The propagators are given as follows:

$$R_{ij} = \epsilon_{lkj}\tfrac{1}{4}(\nabla_k J_{il} - \nabla_l J_{ik}), \quad K_{ijk} = \tfrac{1}{2}(\nabla_k J_{ij} + \nabla_j J_{ik}), \quad (10)$$

where $\boldsymbol{\epsilon}$ is the unit alternating isotropic tensor. When a squirmer is in the far field, high multipoles in Eq. (9) decay very rapidly. So it may be accurate enough to consider only multipoles up to the stresslet, which are obtained as part of the problem in solving Eq. (3). If a squirmer exists in the near field, however, all the multipoles contribute to the ve-

locity field, and one cannot simplify its effect by the first few multipoles. Thus, one needs to calculate a small number of multipoles for squirmers in the far field, but an infinite number of multipoles for squirmers in the near field.

By assuming semidiluteness, Eq. (9) can be approximated as

$$u_i(\boldsymbol{x}) - \langle u_i(\boldsymbol{x})\rangle = \frac{1}{8\pi\mu}\sum_{\alpha=1}^{N}\left[\left(1+\frac{a^2}{6}\nabla^2\right)J_{ij}F_j^\alpha + R_{ij}L_j^\alpha + K_{ijk}S_{jk}^\alpha + \nabla_k\nabla_l J_{ij}Q_{klj}^\alpha\right] - \frac{1}{8\pi\mu}\sum_{\alpha=1}^{N_{near}}\sum_{m=2}^{\infty}{}'\int_{A_\alpha}\left[\frac{(-1)^m}{m!}\frac{\partial^m}{\partial k_1\cdots\partial k_m}J'_{ij} \times (y_{k_1}-x_{k_1}^\alpha)\cdots(y_{k_m}-x_{k_m}^\alpha)q_j(\mathbf{y})\right]dA_y, \quad (11)$$

where N_{near} is the number of squirmers in the near field ($N_{near}\leq 2$) and J'_{ij} is the Oseen tensor given as

$$J'_{ij}(\boldsymbol{r}) = \frac{\delta_{ij}}{r} + \frac{r_i r_j}{r^3}. \quad (12)$$

The contribution from the infinite number of squirmers in the far field is calculated in the first summation on the RHS of Eq. (11). The multipoles exerted on the fluid can be obtained up to the stresslet from Eq. (3), and the irreducible quadrupole is approximated, as explained in [29], as

$$Q_{klj}^\alpha = \left(\frac{a^2}{10}c\langle F_m\rangle + 2\pi\mu a^3 B_1^\alpha e_m^\alpha\right)\left(\delta_{km}\delta_{jl} + \delta_{lm}\delta_{kj} - \frac{2}{3}\delta_{kl}\delta_{jm}\right). \quad (13)$$

The contribution of two squirmers in the near field is calculated by summing up all the multipoles. The first few multipoles are added in the first summation on the RHS of Eq. (11), and the rest of the multipoles are added in the second summation. The prime symbol $'$ on the second sum indicates that the quadrupole contribution already added in the first summation is excluded when $m=2$.

In order to simplify the explanation let $N_{near}=2$, so that two squirmers in the near field interact through an arbitrary linear flow field with a disturbance velocity generated by an infinite number of squirmers in the far field. Considering the linearity of the Stokes flow, the mth multipole exerted on the squirmer in the near field can be divided into four simpler multipoles as schematically shown in Fig. 3: (a) the mth multipole due to translational and rotational motions of two inert spheres in a fluid otherwise at rest; (b) the mth multipole due to the applied linear flow field $\langle \boldsymbol{E}\rangle$, without translational, rotational, and squirming motions; (c) the mth multipole due to squirming motion without translational and rotational motion in a fluid otherwise at rest; and (d) the mth multipole due to the background disturbance flow field generated by the other squirmers in the far field, without translational, rotational, and squirming motions.

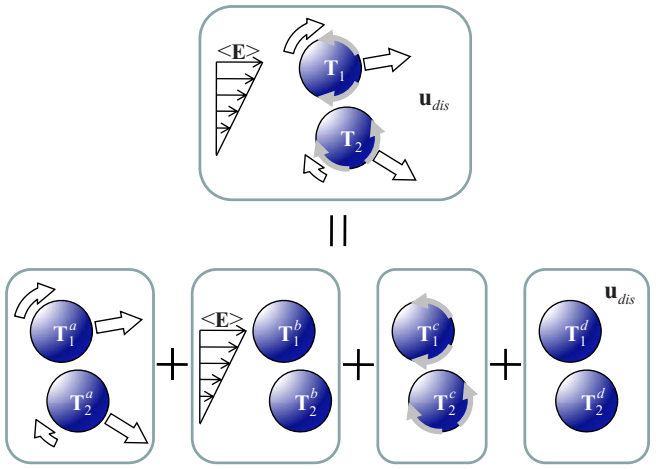

FIG. 3. (Color online) Schematics of superposition of mth multipole $\mathbf{T}$. $\mathbf{T}^a$ is the mth multipole due to the translational-rotational motion, $\mathbf{T}^b$ is due to the applied flow field, $\mathbf{T}^c$ is due to the squirming motion, and $\mathbf{T}^d$ is due to the disturbance flow field $\mathbf{u}_{dis}$ generated by the other squirmers.

The mth multipole in (d), i.e., due to the disturbance flow generated by the other squirmers, can be calculated by the Faxén laws, because the other squirmers are in the far field. The induced multipole decays rapidly, as $r^{-(m+2)}$, where r is the distance, when a squirmer is force free. Since $r^{-(m+2)}$ becomes very small if $m\geq 2$, we can neglect the contribution of (d) for high multipoles. The multipoles in (d) with $m=0,1$, i.e., force, torque, and stresslet, are taken into account, because they are solved as part of the problem in Eq. (3). We should note that the approximated quadrupole given by Eq. (13) is also added in Eq. (11); therefore, part of the contribution from the second multipole is also taken into account. The mth multipole in (a)–(c) can be calculated by considering only two-squirmer interactions, because there is no disturbance flow field generated by the other particles. It is, therefore, computationally efficient to make a database for high multipoles prior to the simulation, so that one needs not to calculate the two squirmer interaction at every time step in the simulation. The database is compiled by a boundary element method, as explained in [28]. The database for $N_{near}=1$ or with a background flow field is straightforward, so the detailed explanation is omitted.

D. Numerical procedures

We will calculate interacting squirmers' motion in a fluid without any imposed flow ($\langle \boldsymbol{E}\rangle=\boldsymbol{0}$) in the three-dimensional space. The maximum volume fraction of squirmers used in this study is 0.15. Note that the probability of a fluid tracer having three or more spheres in its near field is $\mathcal{O}(c^3)$, where c is the volume fraction of squirmers. The computational region is a cube. A suspension of infinite extent is represented by the periodic boundary conditions, and the interaction among an infinite number of particles is calculated by the Ewald summation over two layers on the real- and reciprocal-space lattices. The time marching is performed by the fourth-order Adams–Bashforth scheme with a time step

of 10^{-3}, from random initial positions. In a unit computational domain, we placed 40 squirmers and 60 fluid particles. The effect of particle numbers is checked numerically, and the results are explicitly shown in Sec. III C. The results indicate that the particle number has little effect on the results shown in this paper.

In order to obtain the velocity of a fluid particle, we solve Eq. (11). The computational region is the same cube as for the squirmer motion. In calculating the second summation on the RHS of Eq. (11), we use the database, which was compiled prior to the simulation. In contrast to the database for squirmer motions, where near-field forces are compiled, the single-layer potential distribution on the surface is compiled in this case. This is because the velocity field can be reconstructed from the single-layer potential by integrating it on the surface, and we can considerably reduce the memory size of the database compared to compiling the velocity data in the whole space. The computational mesh for the fluid particle motion may be expressed schematically as shown in Fig. 2(b). When the distance between a fluid particle and a squirmer is larger than r_c, we assume that the squirmer is in the far field. Thus, the computational meshes for particles 3 and 4 in Fig. 2(b) are just points, for which the effect of point singularities is calculated analytically. When the distance between a fluid particle and a squirmer is below r_c, we assume that the squirmer is in the near field. The velocity generated by particles 1 and 2 in Fig. 2(b) is calculated by the BEM. The computational mesh for the BEM is also shown in the figure, in which 590 triangle elements are generated per squirmer surface. A finer mesh is generated in the near-contact region in order to accurately calculate lubrication velocities. In this study, we employed a threshold distance of $r_c=4.0$ for the approximation of far-field interactions. We confirmed numerically that the present far-field approximation is sufficiently accurate when $r>4$, as is discussed explicitly in Secs. III A and III B.

The translational diffusivity is a measure of the increasing displacements between pairs of particles. If the mean-square displacement grows more rapidly than linearly in time, then the spread is superdiffusive, but if it becomes linear in time then the spread is diffusive. Thus, we divide the mean-square displacement by time to see if it becomes constant. The translational displacement is calculated from $\boldsymbol{u}$ as $\boldsymbol{r}=\int \boldsymbol{u}dt$, so the trajectories are traced outside the periodic cell. The translational dispersion tensor $\boldsymbol{D}'$ is defined by

$$\boldsymbol{D}'(\Delta t) = \frac{\langle [\boldsymbol{r}(\Delta t) - \boldsymbol{r}(0)][\boldsymbol{r}(\Delta t) - \boldsymbol{r}(0)] \rangle}{2\Delta t}. \tag{14}$$

The angular brackets $\langle\ \rangle$ indicate an average value over N particles with M different time steps, which is defined as

$$\langle \boldsymbol{r}(\Delta t) - \boldsymbol{r}(0) \rangle = \frac{1}{MN} \sum_{m=1}^{M} \sum_{n=1}^{N} \boldsymbol{r}_n(\Delta t + mdt) - \boldsymbol{r}_n(mdt), \tag{15}$$

where dt is the time step used in the numerical simulation. The diffusion tensor $\boldsymbol{D}$, when it exists, is given by

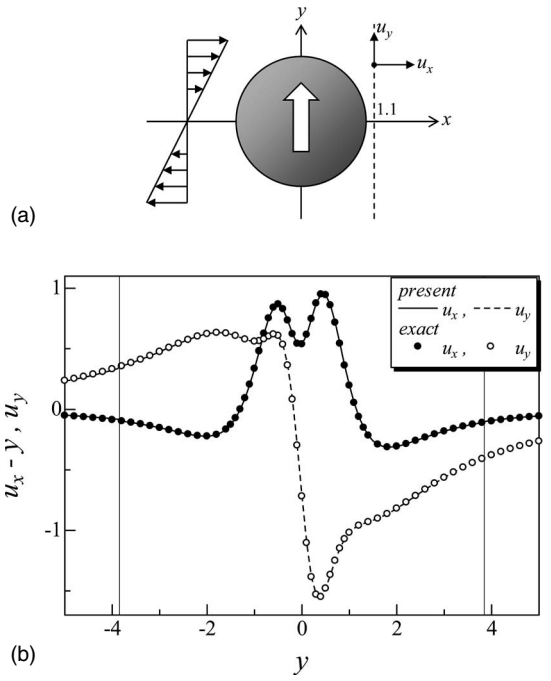

FIG. 4. Velocities around a solitary squirmer with $\beta=5$ swimming in a simple shear flow. The squirmer is orientated in the direction of the velocity gradient, and the shear rate is set equal to a/U_{sol}. (a) Schematic representation of the computed system. (b) Comparison of velocity distribution between the present method (*present*) and the exact solution (*exact*).

$$\boldsymbol{D} = \lim_{\Delta t \to \infty} \boldsymbol{D}'. \tag{16}$$

III. BENCHMARK TESTS OF THE PRESENT NUMERICAL METHODS

In this section, we examine the reliability of the present numerical methods in three different cases: (a) comparison of the velocity field around a solitary squirmer in a simple shear flow between the present methods and the exact solution, (b) comparison of the velocity field around two squirmers in a fluid otherwise at rest between the present methods and BEM, and (c) comparison of the dispersion coefficient of squirmers and fluid particles obtained by the present methods using different particle numbers. In comparison (a), the accuracy of the near- and far-field approximations in the velocity field can be determined. Comparison (b) allows examination of the reliability of the velocity field between two near-contact surfaces. In comparison (c), the effect of the particle number on the dispersion can be determined.

A. Velocity around a solitary squirmer in a simple shear flow

The velocity field around a solitary non-bottom-heavy squirmer with $\beta=5$ in a simple shear flow was compared between the present method and the exact solution. As shown in Fig. 4(a), the squirmer was oriented in the y direction and the shear flow was applied in the x-y plane. The shear rate is set equal to a/U_{sol}, in order to observe the effect

of both squirming and shear velocities. The exact solution was calculated by superimposing the results of Batchelor and Green [46] and those of Ishikawa *et al.* [28]. The solitary squirmer was placed at the origin of coordinates, and x and y components of the velocity were calculated along the $x=1.1$ line. The results for these velocities are shown in Fig. 4(b). We see that the velocities calculated by the present methods agree very well with the exact solution. In this system, the sphere has translational velocity due to the swimming, rotational velocity due to the background vorticity, and squirming velocity on the spherical surface. Moreover, it is placed in the background linear flow field, i.e., a simple shear flow. We can say, therefore, that the present method can accurately calculate the flow field around a sphere with translational, rotational, and squirming motions in a linear flow field.

As explained in Sec. II D, we employed a threshold distance of 4.0 for the approximation of far-field interactions. Thus, the velocity of the present study was calculated differently depending on whether $r>4$ or not. The boundary is shown explicitly in Fig. 4(b) as thin solid lines at $y\approx\pm3.8$. In the near field, the velocity is interpolated from the database compiled by the BEM. The database used in this calculation is the database for translational motion, rotational motion, squirming motion, and background linear flow field. The velocity in the far field was calculated analytically using multipoles up to the stresslet with the approximated quadrupole. Our results confirmed that the near- and far-field approximations match smoothly at $r=4$, and the results are sufficiently accurate.

B. Velocity around two squirmers in a fluid otherwise at rest

The velocity field around two squirmers placed side by side swimming in the opposite direction was compared between the present method and the BEM. As shown in Fig. 5(a), the two squirmers were aligned on the x axis with a gap of 0.2. x and y components of the velocity were calculated along the y axis, and the results are shown in Fig. 5(b). We again employed a threshold distance of 4.0 for the approximation of far-field interactions, and the boundary is shown explicitly in the figure as thin solid lines. We see that the velocities calculated by the present methods and the BEM agreed very well. Although the velocity in the far field was calculated using a small number of multipoles, the results confirmed that the far-field approximation is sufficiently accurate. In the near field, the velocity is interpolated from the database compiled by the BEM. The database used in this calculation is the database for translational, rotational, and squirming motions. The results confirmed that the near-field interpolation is sufficiently accurate even for two squirmers in near contact.

C. Effect of the system size on the diffusivity

To clarify the effects of system size on the diffusivity of squirmers and fluid particles, we performed three trial cases with different particle numbers under the condition of constant volume fraction: (a) 30 squirmers and 50 fluid particles, (b) 40 squirmers and 60 fluid particles, and (c) 50 squirmers and 70 fluid particles. The results with $c=0.1$ and $\beta=5$ are shown in Fig. 6. Since all the curves become horizontal at large enough time, the spreading of squirmers and fluid particles can be correctly described as a diffusive process in all three cases. We see that the differences between the three cases are small. Thus, in the following computations, we placed 40 squirmers and 60 fluid particles per unit computational domain.

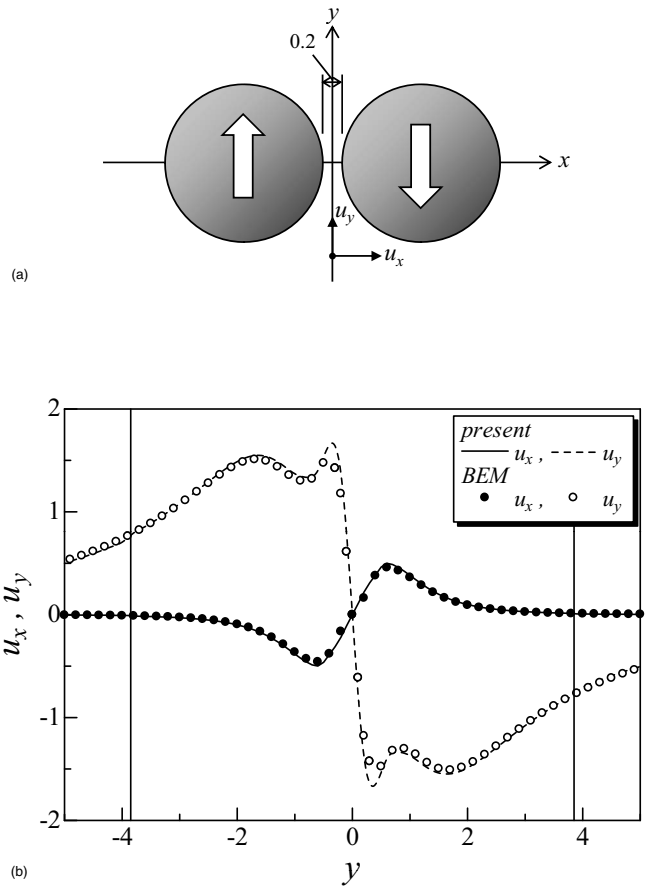

FIG. 5. Velocities around two squirmers with $\beta=5$ swimming in the opposite direction in a fluid otherwise at rest. (a) Schematic representation of the computed system. (b) Comparison of velocity distribution between the present method (*present*) and the boundary element method (*BEM*).

IV. SUSPENSION OF NON-BOTTOM-HEAVY SQUIRMERS

A. Numerical results

In the case of non-bottom-heavy squirmers, there is no preferred orientation. The dispersion tensor of both squirmers and fluid particles should be isotropic, and we will mainly discuss the average of the three diagonal components in the dispersion tensors, defined as $D'=(D'_{xx}+D'_{yy}+D'_{zz})/3$.

The three-dimensional movement of non-bottom-heavy squirmers with $\beta=5$ in a fluid otherwise at rest is computed with volume fraction $c=0.1$. The instantaneous positions of the squirmers and their trajectories over the five previous time intervals are shown in Fig. 7(a). Some of the lines in the figure are not attached to spheres, because a squirmer passing

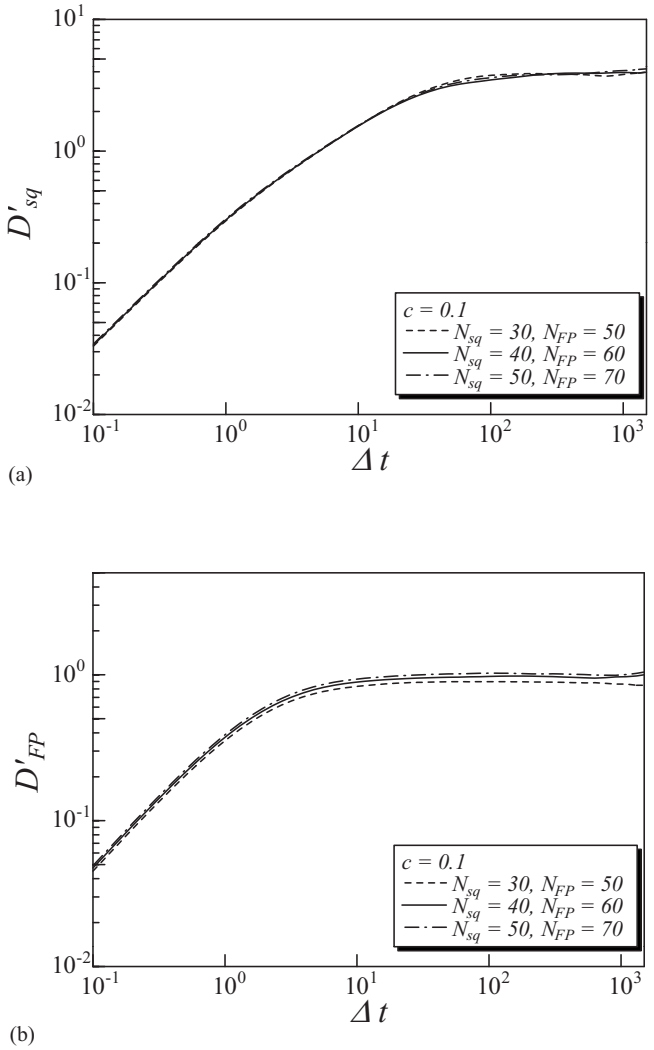

FIG. 6. Effect of particle number on the dispersion coefficient of squirmers and fluid particles, where N_{sq} is the number of squirmers and N_{FP} is the number of fluid particles. The volume fraction c is 0.1, and the squirming mode is β=5. (a) Dispersion of squirmers. (b) Dispersion of fluid particles.

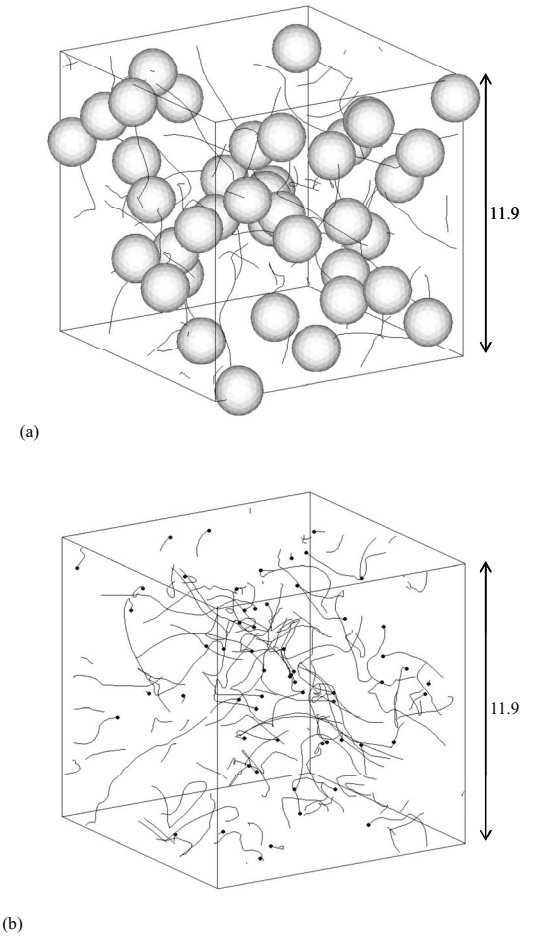

FIG. 7. Motion of squirmers and fluid particles in the case of c=0.1 and β=5. (a) Instantaneous positions of 40 squirmers. Solid lines are trajectories of the squirmers during the five previous time intervals. (b) Instantaneous positions of 60 fluid particles. Solid lines are trajectories of the fluid particles during the five previous time intervals.

through a boundary of the periodic cell is replaced on the other side, and its trajectory has a jump at the boundary. (Note, however, that trajectories for calculating the translational displacement are traced outside the periodic cell.) We see that the trajectories of squirmers are not straight, because the hydrodynamic interaction between squirmers causes them to change direction. The instantaneous positions of the fluid particles and their trajectories over the five previous time intervals are shown in Fig. 7(b). We see that the trajectories of fluid particles are erratic and some of them have long travel distances, as long as those of squirmers. The motion of fluid particles is passively generated by the squirming motions on the spherical surface.

The translational dispersion is calculated from Eq. (14), and the results are shown in Fig. 8 (β=5 and c=0.1). For comparison a line of slope 1 is drawn as well. It is found that the dispersion coefficients of both squirmers and fluid particles converge to constant values D_c if Δt is taken long enough (for squirmers, this result was also found in [47]). Therefore, the spreading of squirmers and fluid particles is correctly described as a diffusive process over a sufficiently long time scale, even though all the movements of the individual particles were deterministic. The diffusivity is larger for squirmers than for fluid particles. The time for particles to show the diffusive property t_c, as indicated in the figure, is longer for squirmers than for fluid particles. This is because the squirmers do not change their directions significantly if they do not experience a near collision.

We also performed additional computations by putting inert spheres of radius a, instead of fluid particles, in the suspension. We put five inert spheres and 59 identical squirmers with β=5 in the computational cell and calculated their motion. The dispersion coefficient for such inert spheres is shown in Fig. 9. We see that such large inert particles also show the diffusive property. We should note that the diffusivity for inert spheres is not less than one tenth of that for fluid particles, even though the particle size is totally different. We have assumed that a fluid particle has no volume, whereas an inert sphere has the same radius as a squirmer. In the case of Brownian diffusion, the diffusivity is inversely

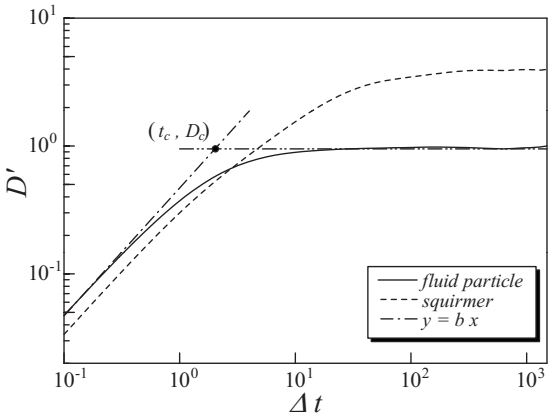

FIG. 8. Dispersion of squirmers and fluid particles during the time interval of Δt (β=5 and c=0.1). Line of slope 1 is drawn for comparison, where the black dot (D_c, t_c) is the intersection of this line and the converged value of D'.

proportional to the particle size. In the case of the diffusion due to cells' swimming motion, however, the effect of particle size is much smaller than for Brownian diffusion. The difference comes from the physical origin of the diffusion; Brownian diffusion is caused by the thermal motion of molecules, whereas the present diffusion is caused by the flow field due to the cells' swimming. The scale of the induced disturbance flow field is very different in these two cases.

The diffusivity of fluid particles and the time for fluid particles to show the diffusive property depend on the volume fraction of squirmers. In order to compare the results effectively, we define the eventual diffusivity D_c and the time scale t_c as shown in Fig. 8. The results for D_c and t_c for squirmers with β=5, fluid particles, and inert spheres are shown in Fig. 10, in which some straight lines are drawn as well for comparison. The error bars in the figure indicate standard error of the mean. Some of the results for squirmers have already been discussed by Ishikawa and Pedley [47], but they are replicated here for comparison. We see that D_c for squirmers decreases approximately as c^{-1}, whereas that for inert spheres increases approximately as c [Fig. 10(a)]. t_c for squirmers decreases approximately as c^{-1}, whereas that for inert spheres is almost independent of c [Fig. 10(b)]. t_c

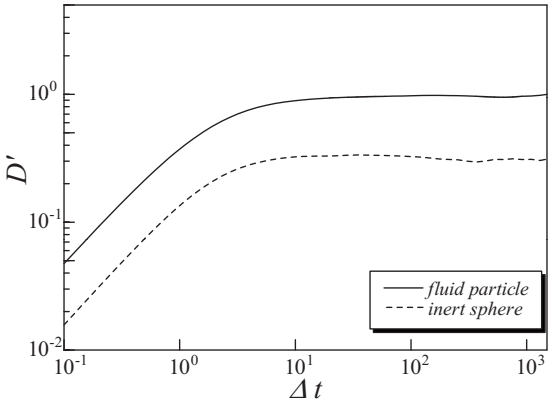

FIG. 9. Dispersion of fluid particles and inert spheres during the time interval of Δt (β=5 and c=0.1).

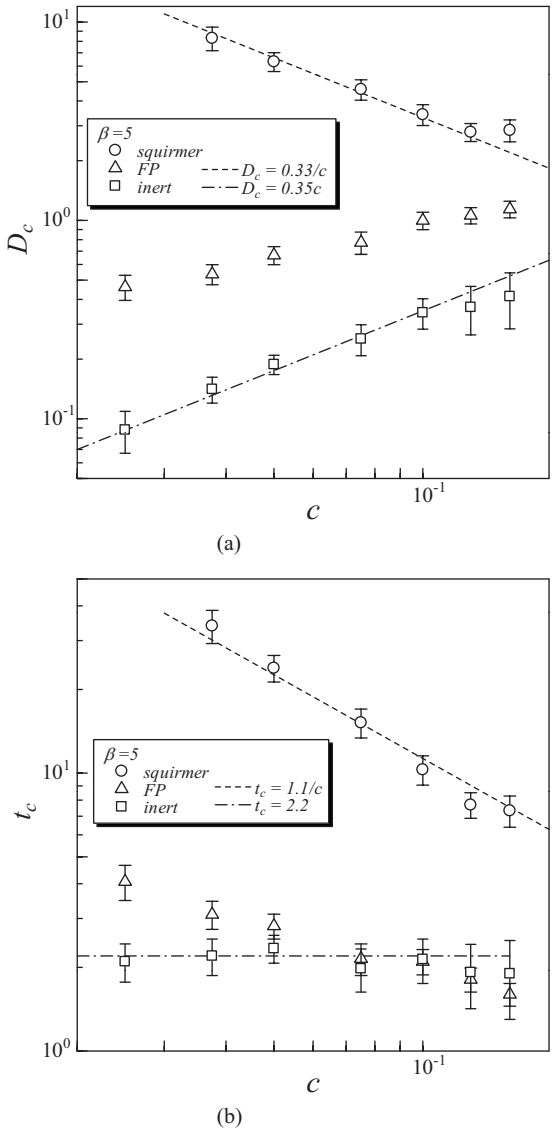

FIG. 10. Effect of c on D_c and t_c (β=5) of fluid particles and inert spheres. *FP* indicates fluid particles, and *inert* indicates inert spheres. Some functions are drawn in the figure for comparison. (a) D_c-c correlation. (b) t_c-c correlation.

for inert spheres is about 2, which is the time scale for a solitary squirmer to swim its body length. The scaling of D_c and t_c for these cases will be discussed in Sec. IV B. In contrast to the inert spheres, the fluid particles show that t_c is slightly decreased as c is increased. In the dilute regime, the fluid particles within the recirculation region around a squirmer may move along with the squirmer until the recirculation region is disturbed by other squirmers. Thus, t_c of the fluid particles is expected to be slightly larger than that of the inert spheres when c is small, which is found in Fig. 10(b).

β is the ratio of second mode squirming to first mode squirming in Eq. (2), i.e., $\beta = B_2/B_1$. Figure 11(a) shows the dispersion of squirmers with $\beta = \pm 1, \pm 5$ (c=0.1). Convergence to a diffusive state was not observed during the time interval $\Delta t \leq 30$ in all cases. However, the dispersion of fluid particles converges to a diffusive state before Δt=10 in all

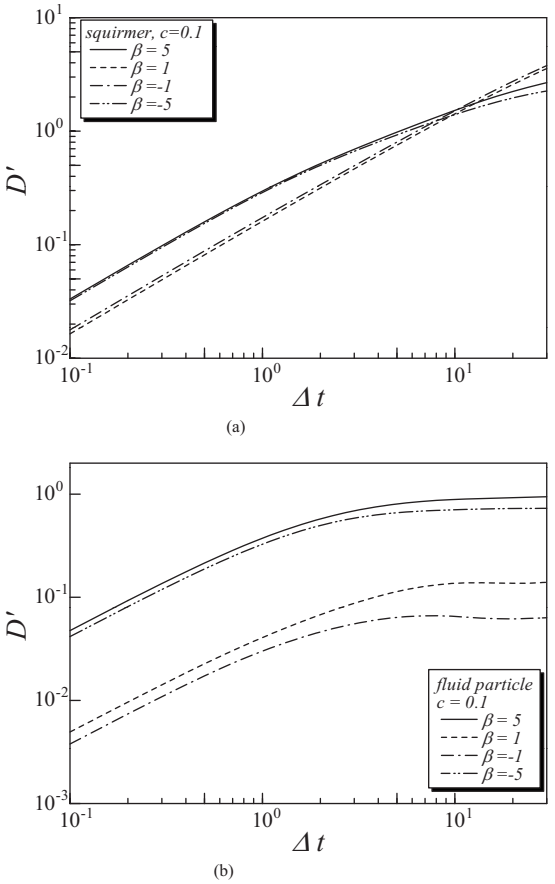

FIG. 11. Effect of β on the diffusivities of squirmers and fluid particles ($c=0.1$). (a) D' of squirmers. (b) D' of fluid particles.

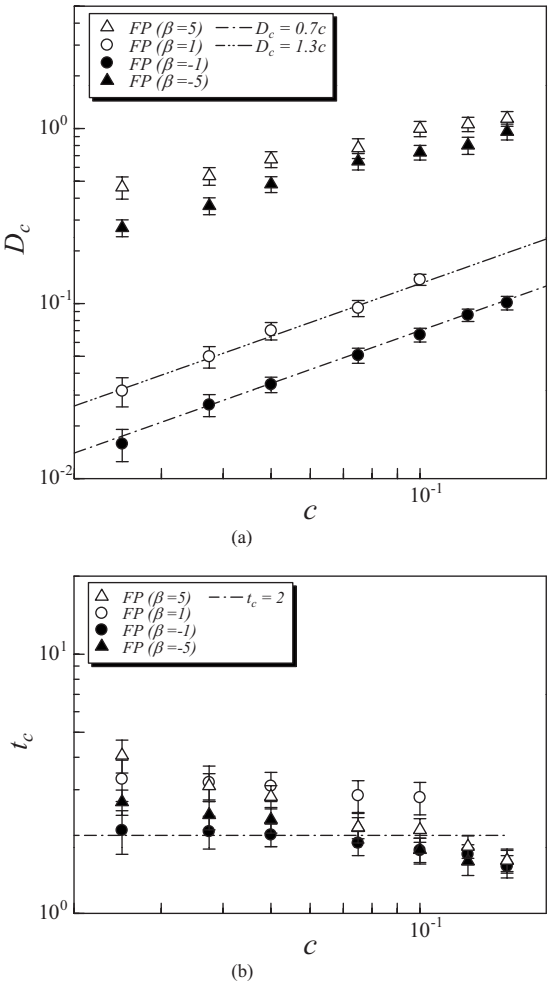

FIG. 12. Effect of β on the c dependence of D_c and t_c. Some functions are drawn in the figure for comparison. (a) D_c-c correlation. (b) t_c-c correlation.

cases [Fig. 11(b)]. The diffusivity increases as the absolute value of β is increased, because squirmers with large β tend to mix up the surrounding fluid considerably. We should note that squirmers with $\beta=\pm 1$ tend to swim in a similar direction and generate ordered coherent structures after a sufficiently long elapsed time (cf. Ishikawa *et al.* [29]). In such a case, the spreading of squirmers is no longer diffusive, and the fluid particles show both advection and diffusion in the suspension. The ordered motion is developed in a time scale of about 200 for $c=0.1$, but it takes a much longer time when the volume fraction of squirmers is small. Before generating the ordered motion, the squirmer motions are erratic, and the spreading of fluid particles becomes diffusive. Here, when $\beta=\pm 1$, we investigated the fluid particle diffusion over a short time scale only, because t_c for fluid particles is about 2. Investigating short time scale diffusion is also convenient to compare our numerical results with the experimental results of Leptos *et al.* [13], in which they measured the short time scale diffusion of the tracer particle in a suspension of *C. reinhardtii*. (The comparison will be shown in Fig. 13.)

The results for D_c and t_c for fluid particles in the $\beta=\pm 5$ and ± 1 cases are shown in Fig. 12, in which some straight lines are drawn as well for comparison. We see that D_c for fluid particles in the $\beta=\pm 1$ case increases as c [Fig. 12(a)], and t_c for fluid particles in the $\beta=\pm 1$ case is almost independent of c [Fig. 12(b)]. These tendencies are similar to the inert sphere case shown in Fig. 10. A squirmer with $\beta=\pm 1$ does not have a recirculation region around it, although a squirmer with $\beta=\pm 5$ does. When a squirmer does not have a recirculation region around it, fluid particles do not move with the squirmer for a long time. Then the scaling of fluid particles in these cases is expected to become similar to that of inert spheres, which is confirmed by comparing Figs. 10 and 12.

Lastly, we discuss the probability density distribution of fluid particles during the diffusion process. Here, we introduce the radial distribution function $g(t,r)$, as in our former study [29]. Mathematically, $ng(t,r)4\pi r^2 dr$ is the average number of particles at time t whose distance from the initial position is between r and $r+dr$, where n is the number density of particles. If the spreading of fluid particles is correctly described as a diffusion process, the distributions at different elapsed times should be self-similar. This is tested by rescaling the length scale from r to $r/t^{1/2}$ and the probability density from $g(r)$ to $g(r)/t^{1/2}$. Figure 13 shows the rescaled plot for the $\beta=5$ case. Since we see that all curves collapse to a narrow-band region, it is confirmed again that the spreading of fluid particles can be correctly described as a diffusion process.

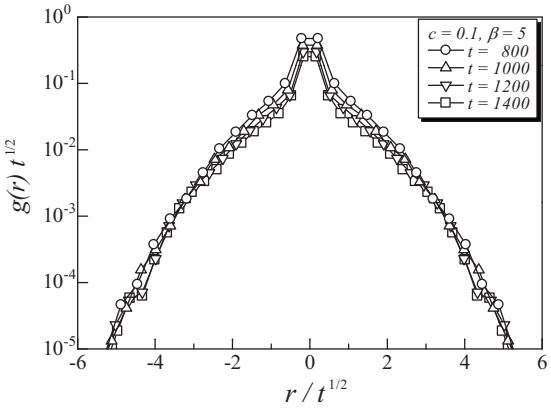

FIG. 13. Time change of radial distribution function, $g(r)$, of tracer particles in suspensions of squirmers ($\beta=5$ and $c=0.1$). Both axes are rescaled by using $t^{1/2}$.

B. Scaling

The scaling for squirmers has already been discussed in [47], so we shall proceed quickly. The diffusivity has a dimension of

$$D_c \propto l_c^2 t_c^{-1} \propto t_c U_c^2, \tag{17}$$

where l_c is the length scale for a squirmer to move in one direction before being reoriented by a close encounter with another squirmer, t_c is the time scale between such encounters, and U_c is the velocity scale of the particle movement. A squirmer swimming at velocity U_{sol} traces out a cylinder of volume $\pi a^2 U_{sol} t$ in time t. When the volume fraction of squirmers is c, the average volume that must be sampled before encountering another squirmer is c^{-1}. So the mean interval t_c between collisions is determined by equating $\pi a^2 U_{sol} t_c = c^{-1}$. By assuming that the swimming velocity is constant, t_c is $\propto c^{-1}$. This tendency is confirmed in Fig. 10(b). D_c can be calculated from Eq. (17) as $D_c \propto c^{-1}$. This tendency also appears in Fig. 10(a).

In contrast to the scalings for squirmers, for inert spheres in the $\beta=5$ case and for fluid particles in the $\beta=\pm 1$ cases with a small elapsed time, it is found that $D_c \propto c$ and t_c is approximately independent of c. In these cases, inert spheres and fluid particles do not move with a squirmer for long distances, so the characteristic velocity scale is not $\mathcal{O}(U_{sol})$. Moreover, the characteristic time scale t_c is not the duration of a mean free path of a squirmer, and a different scaling argument is required. In order to understand the scalings of D_c and t_c for inert spheres and fluid particles, let us consider a simplified model for a fluid particle's random motions. In the dilute regime, an inert sphere or a fluid particle moves along the streamline generated by a nearby squirmer. Since the streamlines around a squirmer are curved, the inert sphere or the fluid particle also follows a curved trajectory, even when the squirmer moves in a straight line. Thus, in the time scale of *collision* to the squirmer, t_{col}, the movement of inert spheres or fluid particles becomes no longer ballistic but rather chaotic. In other words, the motion of inert spheres or fluid particles becomes diffusive in the time scale of t_{col}, and t_c may be approximated as t_{col}. t_{col} can be approximated by the duration for a solitary squirmer to swim its diameter length, i.e., $t_{col}=2a/U_{sol}$, because the velocity field around a squirmer changes considerably in this time scale. Thus, t_c may also be given by $t_c=2a/U_{sol}$. Indeed this is in agreement with the simulation results in Figs. 10(b) and 12(b), i.e., $t_c \approx 2-3$.

Although the movement of inert spheres or fluid particles is not ballistic in the time scale of t_c, the spreading of particles is not governed by this time scale. We need to introduce another time scale to properly explain the diffusion property. Suppose that a collision occurs when a swimmer comes within a certain distance of a fluid particle, and assume that the collision duration t_{col} is much smaller than the mean waiting time t_{wait} between collisions. In a time $t \gg t_{wait}$, a fluid particle experiences on average $n=t/t_{wait}$ collisions. If the displacements arising from successive collisions are uncorrelated, a fluid particle's mean-square displacement is

$$\langle \boldsymbol{r}(t)^2 \rangle = \frac{t}{t_{wait}} \langle \Delta \boldsymbol{x}^2 \rangle. \tag{18}$$

The fluid particle's diffusivity is then

$$D_c = \lim_{t\to\infty} \frac{\langle r(t)^2 \rangle}{6t} = \frac{\langle \Delta \boldsymbol{x}^2 \rangle}{6 t_{wait}}. \tag{19}$$

The frequency of collisions of a fluid particle with squirmers is proportional to the concentration of squirmers, so $1/t_{wait} \propto c$. Since $\Delta \boldsymbol{x}$ is independent of c, D_c becomes proportional to c, in agreement with Figs. 10(a) and 12(a).

The diffusivity of inert particles in a dilute cell suspension was investigated experimentally by Kim and Breuer [12] and Leptos *et al.* [13], although the scaling arguments were not presented. In both experiments, the effective diffusion coefficient in the dilute regime increased linearly as the cell concentration increased. This tendency is consistent with the scaling analysis in this section.

V. SUSPENSION OF BOTTOM-HEAVY SQUIRMERS

In the case of bottom-heavy squirmers, they swim upward on average. The dispersion tensor of both squirmers and fluid particles is no longer isotropic, so we will discuss the vertical and horizontal dispersions separately, which are, respectively, defined as $D_{ver}=D_{yy}$ and $D_{hor}=(D_{xx}+D_{zz})/2$. The gravitational direction is taken as $-\boldsymbol{y}$. In calculating the vertical dispersion, we subtracted off the average vertical velocity of squirmers or fluid particles in the same manner as done by Ishikawa and Pedley [47]. Thus, the vertical dispersion expresses how particles spread relative to their bulk motion. In this study, the average suspension velocity $\langle \boldsymbol{u} \rangle$ in Eq. (3) is set to zero. Therefore, when squirmers swim upward on average, fluid particles flow downward so that the average suspension velocity becomes zero. The accuracy of this treatment is explicitly discussed in the Appendix.

G_{bh} is the ratio of the gravitational torque to a scale for the viscous torque, based on the squirming velocity, as defined by $G_{bh}=(2\pi\rho g a l)/(\mu B_1)$. If one assumes that the micro-organisms swim in water at ten body lengths per sec-

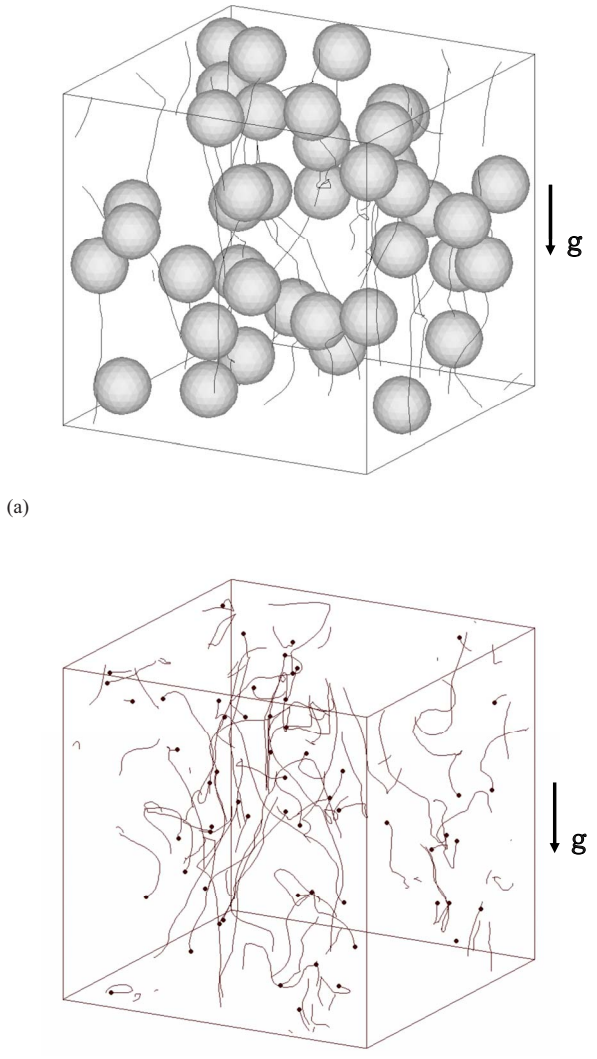

FIG. 14. (Color online) Motion of bottom-heavy squirmers and fluid particles in the case of $G_{bh}=50$, $c=0.1$, and $\beta=5$. (a) Instantaneous positions of 40 bottom-heavy squirmers. Solid lines are trajectories of the squirmers during the five previous time intervals. (b) Instantaneous positions of 60 fluid particles. Solid lines are trajectories of the squirmers during the five previous time intervals.

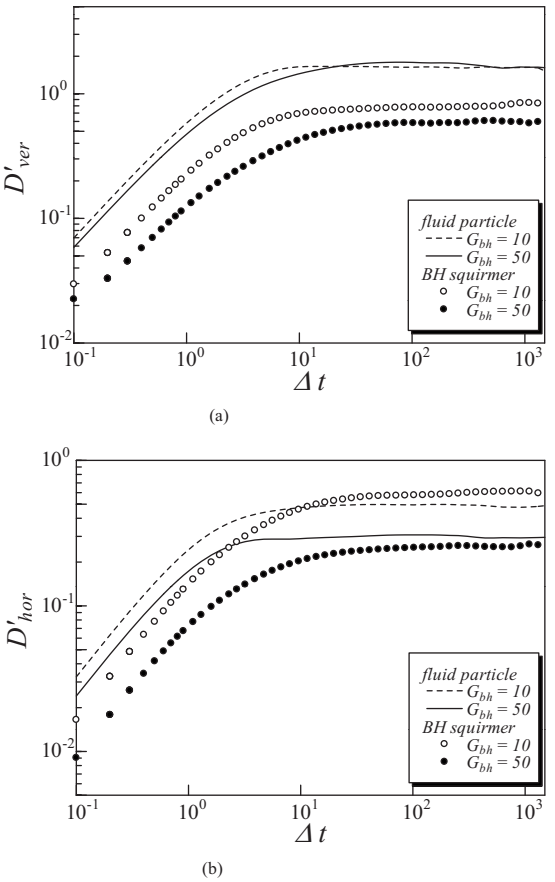

FIG. 15. Effect of G_{bh} on the dispersions of bottom-heavy squirmers and fluid particles ($c=0.1, \beta=5$). (a) Vertical dispersion. (b) Horizontal dispersion.

ond with their center of mass $0.2a$ down from the geometric center, G_{bh} is about 10 for micro-organisms with radius of 25 μm, and about 50 for micro-organisms with radius of 125 μm. The parameter values used in this section are $G_{bh}=10$ and 50.

The movement of bottom-heavy squirmers with $G_{bh}=50$ and $\beta=5$ in a fluid otherwise at rest is computed with volume fraction $c=0.1$. The instantaneous positions of the squirmers and their trajectories over the five previous time intervals are shown in Fig. 14(a). The gravitational direction is shown in the figure as well. We see that the squirmers swim upward on average, but the trajectories are not straight because of the hydrodynamic interaction between squirmers. Figure 14(b) shows the instantaneous positions of the fluid particles and their trajectories over the five previous time intervals. We see that the fluid particles move horizontally as well as vertically, although squirmers swim upward on average.

The vertical dispersions of fluid particles and bottom-heavy squirmers with $G_{bh}=10$ and 50 are calculated, and the results are shown in Fig. 15(a) ($\beta=5$ and $c=0.1$). We see that the vertical dispersion of fluid particles converges to a certain value. Therefore, the vertical spreading of fluid particles relative to their bulk motion is correctly described as a diffusive process over a sufficiently long time scale. The vertical dispersion of fluid particles is larger than that of squirmers. This may be explained by calculating fluid particle motions around a solitary squirmer as follows. Let the center of a solitary squirmer be the origin of the coordinate and let it swim vertically upward, i.e., in the y direction. Initially, 40 fluid particles are placed at $y=4$ with a constant interval in the z direction (Fig. 16). Then, their trajectories over eight time units are calculated, and the results are shown in Fig. 16. We see that the fluid particles spread vertically, although the squirmer swims at a constant velocity. Thus, the solitary squirmer does not show vertical dispersion, but the fluid particles do. Therefore, the dispersion of fluid particles can be larger than that of squirmers in the semidilute regime. The horizontal dispersion of fluid particles is shown in Fig. 15(b). We see that the dispersion coefficients again converge to a constant value. The horizontal diffusivity is considerably lower than the vertical one, because gravity tends to orient

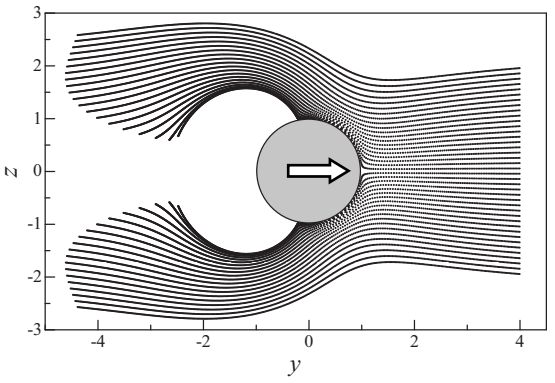

FIG. 16. Trajectories of fluid particles relative to a solitary squirmer with $\beta=5$ swimming in the y direction. Fluid particles are initially placed at $y=4$, and their trajectories are calculated for eight time units. The large arrow in the figure shows the orientation of the solitary squirmer.

the squirmers increasingly in the vertical direction as G_{bh} is increased.

We define $D_{hor,c}$ and $t_{hor,c}$ in a similar manner to D_c and t_c, as explained with respect to Fig. 8, for diffusion in the horizontal direction. The results for $G_{bh}=10,50$ are shown in Fig. 17 ($\beta=5$), in which some straight lines are drawn as well for comparison. In the case of the horizontal diffusivity of fluid particles, the effect of the recirculation region behind a squirmer is small, because a fluid particle does not move horizontally even if it resides in the recirculation region. In such a case, the scaling of diffusive properties may be similar to that of inert spheres. We see from Fig. 17 that $D_{hor,c}$ with $G_{bh}=10$ and 50 is approximately proportional to c and $t_{hor,c}$ is roughly independent of c. These tendencies are the same as for inert spheres in a suspension of non-bottom-heavy squirmers (cf. Fig. 10).

In order to emphasize the effect of bottom heaviness, the change in $D_{hor,c}$ with G_{bh} is shown in Fig. 18. (When $G_{bh}=0$, $D_{hor,c}$ is equivalent to D_c.) It is found that $D_{hor,c}$ decreases considerably even with small values of G_{bh}, which indicates the importance of bottom heaviness in the horizontal diffusion. When G_{bh} is large, $D_{hor,c}$ of squirmers becomes even smaller than that of fluid particles. Under such a condition, mass transport in the horizontal direction is mainly mediated by the mixing due to swimming motions of microorganisms, not by the ballistic locomotion of cells.

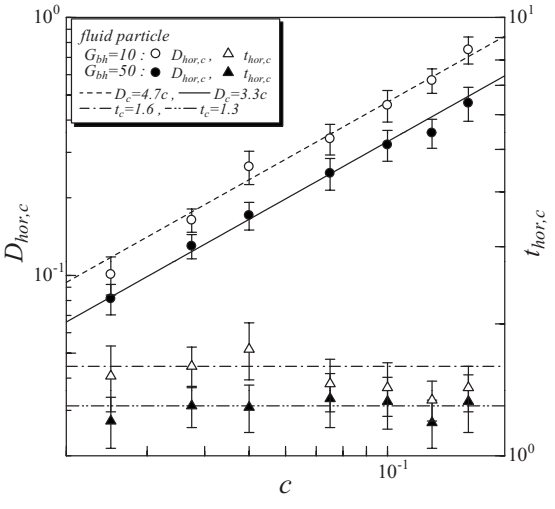

FIG. 17. Effect of bottom heaviness on the diffusive properties of fluid particles in the horizontal direction ($G_{bh}=10$ and 50, $\beta=5$). Some functions are drawn in the figure for comparison.

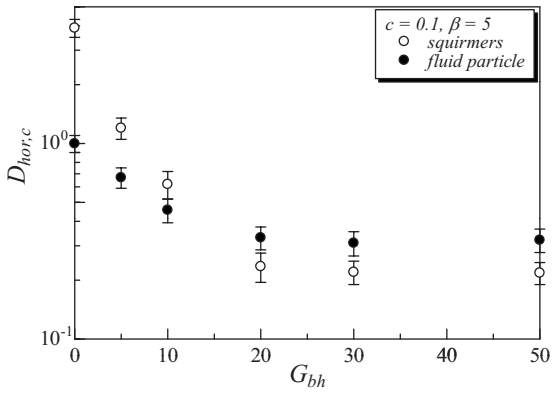

FIG. 18. Effect of G_{bh} on the horizontal diffusivity ($c=0.1$ and $\beta=5$).

VI. CONCLUSIONS

We have calculated fluid particle diffusion in a semidilute suspension of squirmers. Squirmer motions in an infinite suspension otherwise at rest were computed by the Stokesian-dynamics method. For the fluid particle motions, we proposed a numerical method based on a combination of the boundary element and Stokesian-dynamics methods. We presented details of the numerical method and confirmed its accuracy.

The computational results show that the spreading of squirmers and fluid particles is correctly described as a diffusive process, even though all the movements of the individual particles are deterministic. In the case of a suspension of non-bottom-heavy squirmers with $\beta=5$, the diffusivity of fluid particles is smaller than that of squirmers. The time scale for convergence to diffusive behavior is shorter for fluid particles than for squirmers. The effect of the size of tracer particles was also investigated by putting some inert spheres, instead of fluid particles, into the suspension. The diffusivity for inert spheres is not less than one tenth of that for fluid particles, even though the particle size is totally different. These tendencies are very different from Brownian diffusion, which can be explained by the difference in the physical origin of the diffusion.

The effect of swimming mode β on the fluid particle diffusion is also investigated for a small elapsed time. The probability density distribution of fluid particles in the $\beta=1$ case becomes non-Gaussian but shows exponential (Laplace) distribution. This tendency shows good agreement with the experimental results of a suspension of *C. reinhardtii* [13].

The scaling analysis of inert spheres in the $\beta=5$ case and of fluid particles in the $\beta=\pm 1$ case shows that D_c is proportional to c, whereas t_c is independent of c. These scalings

match well with the numerical results, provided that the effect of the recirculation region is small. In the case of a suspension of bottom-heavy squirmers, the fluid particles again show diffusive behavior. The horizontal spreading of fluid particles shows that D_c is proportional to c and t_c is roughly independent of c. $D_{hor,c}$ decreases considerably even with small values of G_{bh}, which indicates the importance of bottom heaviness in the horizontal diffusion. We believe that these fundamental findings will enhance our understanding of the basic mechanics of a suspension of swimming microorganisms.

ACKNOWLEDGMENTS

We are grateful for discussions with R. E. Goldstein, J. P. Gollub, and K. Leptos. We are grateful for financial support of the Japan Society for the Promotion of Science (Grant-in-Aid for Young Scientists No. 19686016 to T.I.), the Royal Society of London (International Joint Project Grant for T.J.P. and T.I.), and the University of Cambridge (Oliver Gatty Grant for J.T.L.).

APPENDIX: ACCURACY OF THE AVERAGE SUSPENSION VELOCITY

The aim of this appendix is to clarify the accuracy of the average suspension velocity obtained by the present numerical method. Since the velocities of individual particles are calculated by the Stokesian-dynamics method, the average particle velocity can be easily obtained by averaging them over all particles and many time steps. In order to obtain the average velocity of the fluid phase, on the other hand, one needs to calculate quite a large number of fluid particles homogeneously distributed in the suspension. This averaging procedure in fluid velocity may introduce additional numerical error.

In order to avoid such an error, we first calculate sedimentation velocity of a simple cubic array of identical spheres defined relative to zero-volume flux axes, i.e., such that the average suspension velocity is zero. The exact solution of this problem was derived by Zick and Homsy [48]. A similar discussion can be found in [34], but we reproduce it in order for readers to confirm the accuracy. Figure 19 shows the nondimensional sedimentation velocity obtained by the present method and the exact solution. We see that the two results agree well even in the high volume fraction regime, which indicates that the sedimentation velocity is accurately calculated in the frame of zero-volume flux by the present method.

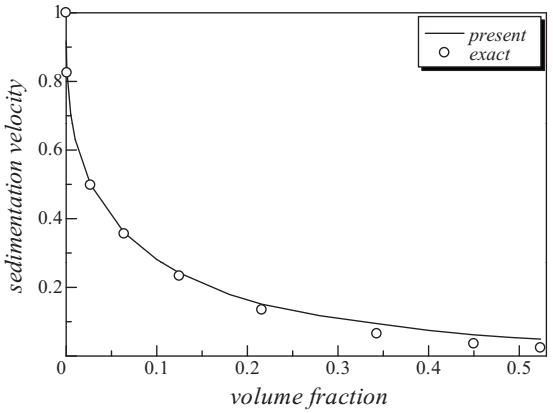

FIG. 19. Nondimensional sedimentation velocity of a simple cubic array of identical spheres defined relative to zero-volume flux axes. *Present* indicates the results obtained by the present method, and *exact* indicates the exact solution of Magar and Pedley [40].

We also calculated the average squirmer velocity $\langle U_{y,sq}\rangle$ and the average fluid particle velocity $\langle U_{y,fp}\rangle$ for the cases $G_{bh}=10$ and 50, shown in Fig. 15. The velocities are averaged over 250 time units and 40 squirmers or 60 fluid particles. When $G_{bh}=10$, $\langle U_{y,sq}\rangle=0.64$ and $\langle U_{y,fp}\rangle=-0.069$. The suspension average velocity $\langle U_y\rangle$ can be calculated by $\langle U_y\rangle = c\langle U_{y,sq}\rangle+(1-c)\langle U_{y,fp}\rangle$, where c is the volume fraction. By substituting $c=0.1$, $\langle U_y\rangle$ of $G_{bh}=10$ becomes 0.002. Since the average suspension velocity is zero, $\langle U_y\rangle$ is expected to be zero. Similarly, $\langle U_{y,sq}\rangle$, $\langle U_{y,fp}\rangle$, and $\langle U_y\rangle$ for the $G_{bh}=50$ case are calculated as 0.90, −0.14, and 0.036, respectively. The error in $\langle U_y\rangle$ increases with G_{bh}, because the relative velocity between the particle and the fluid increases. Although we could not avoid the small error in averaging the fluid velocity, the accuracy of zero-volume flux is acceptable even for a suspension of bottom-heavy squirmers.

[1] T. Ishikawa, J. R. Soc., Interface **6**, 815 (2009).
[2] M. J. R. Fasham, H. W. Ducklow, and S. M. McKelvie, J. Mar. Res. **48**, 591 (1990).
[3] T. J. Pedley and J. O. Kessler, Annu. Rev. Fluid Mech. **24**, 313 (1992).
[4] A. M. Metcalfe, T. J. Pedley, and T. F. Thingstad, J. Mar. Syst. **49**, 105 (2004).
[5] S. Childress, M. Levandowsky, and E. A. Spiegel, J. Fluid Mech. **69**, 591 (1975).
[6] T. J. Pedley and J. O. Kessler, J. Fluid Mech. **212**, 155 (1990).
[7] A. J. Hillesdon, T. J. Pedley, and J. O. Kessler, Bull. Math. Biol. **57**, 299 (1995).
[8] M. A. Bees and N. A. Hill, Phys. Fluids **10**, 1864 (1998).
[9] A. M. Metcalfe and T. J. Pedley, J. Fluid Mech. **445**, 121 (2001).
[10] N. A. Hill and T. J. Pedley, Fluid Dyn. Res. **37**, 1 (2005).
[11] X.-L. Wu and A. Libchaber, Phys. Rev. Lett. **84**, 3017 (2000).
[12] M. J. Kim and K. S. Breuer, Phys. Fluids **16**, L78 (2004).
[13] K. C. Leptos, J. S. Guasto, J. P. Gollub, A. I. Pesci, and R. E. Goldstein, Phys. Rev. Lett. **103**, 198103 (2009).
[14] J. P. Hernandez-Ortiz, C. G. Stoltz, and M. D. Graham, Phys. Rev. Lett. **95**, 204501 (2005).
[15] P. T. Underhill, J. P. Hernandez-Ortiz, and M. D. Graham, Phys. Rev. Lett. **100**, 248101 (2008).
[16] D. Saintillan and M. J. Shelley, Phys. Rev. Lett. **100**, 178103 (2008).

[17] D. Saintillan and M. J. Shelley, Phys. Fluids **20**, 123304 (2008).
[18] I. Llopis and I. Pagonabarraga, EPL **75**, 999 (2006).
[19] I. Llopis and I. Pagonabarraga, Eur. Phys. J. E **26**, 103 (2008).
[20] A. J. C. Ladd, J. Fluid Mech. **271**, 285 (1994).
[21] A. J. C. Ladd, J. Fluid Mech. **271**, 311 (1994).
[22] A. J. C. Ladd, Phys. Fluids **9**, 491 (1997).
[23] A. S. Sangani and G. Mo, Phys. Fluids **8**, 1990 (1996).
[24] A. Z. Zinchenko and R. H. Davis, J. Comput. Phys. **157**, 539 (2000).
[25] A. Z. Zinchenko and R. H. Davis, J. Fluid Mech. **455**, 21 (2000).
[26] A. Z. Zinchenko and R. H. Davis, J. Comput. Phys. **207**, 695 (2005).
[27] A. Z. Zinchenko and R. H. Davis, J. Comput. Phys. **227**, 7841 (2008).
[28] T. Ishikawa, M. P. Simmonds, and T. J. Pedley, J. Fluid Mech. **568**, 119 (2006).
[29] T. Ishikawa, J. T. Locsei, and T. J. Pedley, J. Fluid Mech. **615**, 401 (2008).
[30] T. Ishikawa and T. J. Pedley, Phys. Rev. Lett. **100**, 088103 (2008).
[31] J. C. M. Li and P. Chang, J. Chem. Phys. **23**, 2012 (1955).
[32] T. Ishikawa and T. Yamaguchi, Phys. Rev. E **77**, 041402 (2008).
[33] J. F. Brady and G. Bossis, Annu. Rev. Fluid Mech. **20**, 111 (1988).
[34] J. F. Brady, R. J. Phillips, J. C. Lester, and G. Bossis, J. Fluid Mech. **195**, 257 (1988).
[35] M. J. Lighthill, Commun. Pure Appl. Math. **5**, 109 (1952).
[36] J. R. Blake, J. Fluid Mech. **46**, 199 (1971).
[37] B. U. Felderhof and R. B. Jones, Physica A **202**, 119 (1994).
[38] H. A. Stone and A. D. T. Samuel, Phys. Rev. Lett. **77**, 4102 (1996).
[39] V. Magar, T. Goto, and T. J. Pedley, Q. J. Mech. Appl. Math. **56**, 65 (2003).
[40] V. Magar and T. J. Pedley, J. Fluid Mech. **539**, 93 (2005).
[41] C. W. J. Beenakker, J. Chem. Phys. **85**, 1581 (1986).
[42] L. Durlofsky, J. F. Brady, and G. Bossis, J. Fluid Mech. **180**, 21 (1987).
[43] S. Kim and S. J. Karrila, *Microhydrodynamics: Principles and Selected Applications* (Butterworth Heinemann, London, 1992).
[44] J. F. Brady and G. Bossis, J. Fluid Mech. **155**, 105 (1985).
[45] C. Pozrikidis, *Boundary Integral and Singularity Methods for Linearized Viscous Flow* (Cambridge University Press, Cambridge, England, 1992), Chap. 4.
[46] G. K. Batchelor and J. T. Green, J. Fluid Mech. **56**, 375 (1972).
[47] T. Ishikawa and T. J. Pedley, J. Fluid Mech. **588**, 437 (2007).
[48] A. Zick and G. M. Homsy, J. Fluid Mech. **115**, 13 (1982).